

同行专家业内评价意见书编号：20250858232

附件1

浙江工程师学院（浙江大学工程师学院） 同行专家业内评价意见书

姓名： 蔡一晟

学号： 22260118

申报工程师职称专业类别（领域）： 能源动力

浙江工程师学院（浙江大学工程师学院）制

2025年03月20日

填表说明

一、本报告中相关的技术或数据如涉及知识产权保护、军工项目保密等内容，请作脱密处理。

二、请用宋体小四字号撰写本报告，可另行附页或增加页数，A4纸双面打印。

三、表中所涉及的签名都必须用蓝、黑色墨水笔，亲笔签名或签字章，不可以打印代替。

四、同行专家业内评价意见书编号由工程师学院填写，编号规则为：年份4位+申报工程师职称专业类别(领域)4位+流水号3位，共11位。

一、个人申报

(一) 基本情况【围绕《浙江工程师学院（浙江大学工程师学院）工程类专业学位研究生工程师职称评审参考指标》，结合该专业类别(领域)工程师职称评审相关标准，举例说明】

1. 对本专业基础理论知识和专业技术知识掌握情况(不少于200字)

熟练掌握本专业的基础理论知识，包括电力工程基础、电力系统稳态及暂态分析、电力电子技术、发电厂电气部分以及新能源发电变流技术等，熟悉各种专业知识技术，如电力系统潮流分析、电力系统暂态稳定分析、电力系统模型构建等，并能够采用PSCAD、MATLAB/Simulink等软件进行电力系统的仿真与分析工作；对目前电力系统行业的工程难题及学术前沿有着深刻的了解和认知，能够利用掌握的专业知识和技能对实际问题进行分析，并通过仿真和实验等方式进行验证，最终解决实际工程问题。

2. 工程实践的经历(不少于200字)

在专业实践中，我有机会亲自操作了多种先进的电网监测设备，包括RT-LAB等半实物仿真器件。这些设备在实际工程中至关重要，通过它们，我深刻理解了如何将所提方法应用到实际生产中的流程和技术要求。此外，我还掌握了多个专业软件的使用方法，如Matlab/Simulink、PSCAD等进行了详尽的系统建模仿真和数据分析处理。在操作这些软件时，我不仅熟悉了其功能和使用方法，更通过多次实验和模拟验证了各种理论模型在实际工程中的可行性。这些实际操作经验让我掌握了最前沿的电网技术和工具，大大增强了我解决复杂工程问题的能力。我不仅能够将课堂上学习的理论知识应用于实践中，还能在实际项目中灵活应对各种挑战，提出切实可行的解决方案，从而显著提升了我在电气工程领域的综合应用能力。

3. 在实际工作中综合运用所学知识解决复杂工程问题的案例(不少于1000字)

随着全球能源结构的转型，风电、光伏等新能源发电在电力系统中的占比不断提高。根据国家能源局发布的统计数据，截至2024年10月底，全国风电、光伏装机容量累计约占全部装机容量的40%，且新增装机容量中风电、光伏占比高达81.3%。然而，新能源发电设备与传统同步发电机相比，缺乏惯量和阻尼特性，导致电力系统面临惯量支撑不足、频率稳定性下降等问题。特别是在海上风电经柔性直流输电外送系统中，新能源发电设备的占比增加，系统的暂态同步稳定性问题尤为突出。本案例旨在量化研究含构网型风机海上风电柔直外送系统的暂态同步稳定性，通过简化系统模型、提出临界切除时间计算方法，并结合仿真验证，解决实际电力系统设计和运行中的复杂工程问题。

在海上风电经柔直外送系统中，构网型和跟网型新能源变流器协同工作时，系统的暂态同步稳定性变得复杂。构网型新能源能够提供惯量和阻尼支撑，但也会引入功角振荡和同步稳定问题。如何准确量化系统的暂态稳定性，确保系统在故障情况下的稳定运行，成为实际工程中的一大难题。为了解决这一问题，首先，以我国南部沿海某实际电网作为算例系统，并对系统进行简化，分析其交互耦合机理。系统主要由构网型风机、跟网型风机和柔性直流输电系统组成。构网型风机采用虚拟同步机控制策略，模拟同步发电机的惯量和阻尼特性；跟网型风机则采用传统的功率控制策略，通过锁相环实现与电网的同步。通过时间尺度划分，忽略对分析结果影响较小的快动态过程，简化系统模型。构网型风机和柔性直流换流站被等效为受控电压源，跟网型风机被等效为受控电流源，接着推导系统的节点电流方程和等效转子运动方程，为后续的暂态稳定性分析奠定了基础。

为了量化系统的暂态稳定性，提出了考虑电压动态特性和阻尼的临界切除时间计算方法。首先，基于故障初值近似，计算故障中各变量的初始值。然后，通过等面积定则计算临界切除角的初值，并结合电压动态特性进行修正，确保计算结果的保守性。具体步骤包括计算故障

前后系统各变量的平衡点值，计算故障初始时刻构网型、跟网型风机和柔性直流换流站的电压幅值、相角及跟网型风机的输出电流角，计算故障中和故障后的功率耦合项、等效参考功率、等效输出功率和阻尼项面积，根据等面积定则计算考虑阻尼影响的临界切除角初值，结合电压动态特性修正故障切除后的电压值，重新计算临界切除角，最后根据临界切除角推导临界切除时间的解析表达式。

在Matlab/Simulink平台中搭建仿真模型，验证所提方法的有效性。通过设置不同的故障场景，验证临界切除时间和临界切除角的准确性。仿真结果表明，所提方法能够准确判断系统的暂态稳定性，且在多个场景下与时域仿真结果的平均误差仅为-

2.63%。此外，分析了等效惯量、阻尼系数、无功电流系数等参数对系统暂态同步稳定性的影响。结果表明，增大等效惯量和阻尼系数能够抑制故障时的角频率变化，提高系统的稳定性；增大无功电流系数有利于减小故障中的加速面积，增大无功电压系数能够同时增大减速面积和减少加速面积，从而改善系统的暂态同步稳定性。

本案例所提出的方法在实际工程中具有广泛的应用前景。首先，该方法能够为海上风电经柔直外送系统的设计和运行提供理论依据，确保系统在故障情况下的稳定运行。其次，通过量化系统的暂态稳定性，能够为继电保护装置的参数整定提供参考，提高系统的可靠性和安全性。通过对系统参数的优化调整，显著提高了系统的暂态同步稳定性，确保了风电的高效外送和电网的稳定运行。

通过本案例的实施，不仅解决了复杂的工程问题，还积累了宝贵的经验，为今后类似工程项目的实施提供了参考和借鉴。本案例通过简化系统模型、提出临界切除时间计算方法，并结合仿真验证，成功解决了海上风电经柔直外送系统的暂态同步稳定性问题。所提方法在保证准确性和保守性的同时，极大提高了暂态稳定分析的效率，具有较高的工程应用价值。未来，该方法可进一步推广至其他新能源发电系统的稳定性分析中，为电力系统的安全稳定运行提供有力支持。

(二) 取得的业绩(代表作)【限填3项, 须提交证明原件(包括发表的论文、出版的著作、专利证书、获奖证书、科技项目立项文件或合同、企业证明等)供核实, 并提供复印件一份】

1. 公开成果代表作【论文发表、专利成果、软件著作权、标准规范与行业工法制定、著作编写、科技成果获奖、学位论文等】

成果名称	成果类别 [含论文、授权专利(含发明专利申请)、软件著作权、标准、工法、著作、获奖、学位论文等]	发表时间/授权或申请时间等	刊物名称/专利授权或申请号等	本人排名/总人数	备注
Rapid Estimation of CCT for GFM and GFL Inverters Integrated Systems Using the Direct Method	会议论文	2024年12月02日	the 8th IEEE Conference on Energy Internet and Energy System Integration	1/4	
一种跟网型与构网型变流器并联系统的主导不稳定平衡点求解方法	发明专利申请	2024年05月30日	申请号: 2024106883897	2/8	

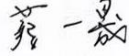
2. 其他代表作【主持或参与的课题研究项目、科技成果应用转化推广、企业技术难题解决方案、自主研发设计的产品或样机、技术报告、设计图纸、软课题研究报告、可行性研究报告、规划设计方案、施工或调试报告、工程实验、技术培训教材、推动行业发展中发挥的作用及取得的经济社会效益等】

(三) 在校期间课程、专业实践训练及学位论文相关情况

课程成绩情况	按课程学分核算的平均成绩： 87 分
专业实践训练时间及考核情况(具有三年及以上工作经历的不作要求)	累计时间： 1 年(要求1年及以上) 考核成绩： 83 分

本人承诺

个人声明：本人上述所填资料均为真实有效，如有虚假，愿承担一切责任，特此声明！

申报人签名： 

浙江大学研究生院
攻读硕士学位研究生成绩单

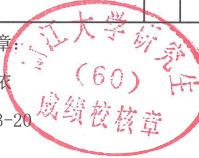
学号: 22260118	姓名: 蔡一晟	性别: 男	学院: 工程师学院	专业: 电气工程	学制: 2.5年						
毕业时最低应获: 24.0学分	已获得: 28.0学分			入学年月: 2022-09	毕业年月:						
学位证书号:			毕业证书号:			授予学位:					
学习时间	课程名称	备注	学分	成绩	课程性质	学习时间	课程名称	备注	学分	成绩	课程性质
2022-2023学年秋季学期	新时代中国特色社会主义思想理论与实践		2.0	90	专业学位课	2022-2023学年秋冬学期	工程管理		2.0	85	跨专业课
2022-2023学年秋季学期	工程技术创新前沿		1.5	85	专业学位课	2022-2023学年春季学期	自然辩证法概论		1.0	89	专业学位课
2022-2023学年秋季学期	新能源发电与变流技术		2.0	96	专业学位课	2022-2023学年春季学期	电气装备健康管理		2.0	85	专业选修课
2022-2023学年冬季学期	产业技术发展前沿		1.5	96	专业学位课	2022-2023学年春季学期	高阶工程认知实践		3.0	89	专业学位课
2022-2023学年秋冬学期	数据分析的概率统计基础		3.0	85	专业选修课	2022-2023学年夏季学期	研究生英语		2.0	免修	专业学位课
2022-2023学年秋冬学期	研究生论文写作指导		1.0	87	专业选修课	2022-2023学年夏季学期	研究生英语基础技能		1.0	免修	公共学位课
2022-2023学年冬季学期	综合能源系统集成优化		2.0	89	专业学位课		硕士生读书报告		2.0	通过	
2022-2023学年秋冬学期	工程伦理		2.0	83	专业学位课						

说明: 1. 研究生课程按三种方法计分: 百分制, 两级制 (通过、不通过), 五级制 (优、良、中、及格、不及格)。
2. 备注中 "*" 表示重修课程。

学院成绩校核章:

成绩校核人: 张梦依

打印日期: 2025-03-20



Rapid Estimation of CCT for GFM and GFL Inverters Integrated Systems Using the Direct Method

1st Yisheng Cai

Zhejiang University

Provincial Key Laboratory of Renewable Energy

Electrical Technology and Systems

Hangzhou, China

22260118@zju.edu.cn

2nd Zhichao Gong

Zhejiang University

Provincial Key Laboratory of Renewable Energy

Electrical Technology and Systems

Hangzhou, China

22460289@zju.edu.cn

3rd Wenqi Huang

New Energy System Research Institute

China Southern Power Grid

Beijing, China

huangwq@csg.cn

4th Yongzhi Zhou

Zhejiang University

Provincial Key Laboratory of Renewable Energy

Electrical Technology and Systems

Hangzhou, China

zhouyongzhi@zju.edu.cn

Abstract—The integration of grid-forming (GFM) inverters can provide voltage and frequency support for the system and enhance system stability. However, existing transient stability analyses for GFM and grid-following (GFL) inverters integrated systems face challenges in rapidly estimating the stability domain, limiting their suitability for online applications. To address these issues, this paper quantifies the system's transient stability domain using the critical clearing time (CCT). By considering the Q-V characteristics of the GFM and the power output characteristics of the GFL, the structure-preserving transient energy function (TEF) is derived based on the energy conservation law. Then, an improved iterative potential energy boundary surface (IPEBS) method is proposed to evaluate the CCT, which reduces estimation errors and prevents misjudgments while ensuring a conservative CCT estimation. Finally, simulations verify the method's efficiency, accuracy, and conservatism.

Index Terms—CCT, direct method, TEF, IPEBS, grid-following (GFL), grid-forming (GFM).

I. INTRODUCTION

The adoption of low-carbon energy is imperative, necessitating the integration of substantial renewable energy and supporting resources—including wind turbines, solar arrays, battery storage, and fuel cells—into the power system, primarily through power electronic inverters [1], [2]. Within power electronic inverter technology, grid-Forming (GFM) and grid-following (GFL) inverters are predominantly utilized [3]. GFM inverters control the AC side voltage and facilitate the formation of a voltage source grid, synchronizing with the rest of the grid through frequency droop control [4]. In contrast, GFL inverters manage the current on the AC side and track the phase angle of the existing grid voltage using a phase-locked loop (PLL). However, questions remain regarding the effective integration of GFM and GFL inverters, especially in transient situations.

Commonly used methods for analyzing transient stability include time-domain simulation and direct methods [5], a study examined the influence of the phase angle of GFL-injected current on GFM transient synchronization stability under varying line impedances [6]. The transient stability of power systems co-dominated by different types of GFM devices has been investigated [7]. The interaction among the GFM and GFL converters operating nearby was analyzed and addressed in Ref. [8]. Further research compared the transient energy functions of GFM and GFL systems, analyzing how system parameters affect transient stability and deriving stability boundaries under large disturbances [9]. Another research quantified the impact of GFM access on enhancing system stability from the perspective of small disturbance stabilization and proposes a capacity allocation method aimed at improving the SCR [10].

In summary, existing research continues to face challenges in rapidly estimating the stability domain and accurately quantifying the Q-V characteristics of GFM inverters and the internal dynamics of GFL inverters, which limits its application for online systems. This paper addresses these challenges with the following contributions:

1) A TEF for the system based on energy conservation law is derived, incorporating the Q-V characteristics of the GFM inverter and the power output characteristics of the GFL inverter as potential energy components;

2) An improved IPEBS method is proposed, which minimizes potential excessive CCT estimation errors of the traditional IPEBS method;

3) The proposed TEF is verified through theoretical proofs and simulations, while the validity of the improved IPEBS method are confirmed across different operational scenarios.

The remainder of this paper is organized as follows. Section II derives the system's TEF, Section III presents the CCT evaluation using the improved IPEBS method. Section IV presents simulation results and comparative analysis. Section V concludes the paper.

II. DERIVATION OF THE TEF

A. System Modelling

For generality, the GFM inverter implement virtual synchronous generator (VSG) control [11], the per unit mathematical model is described as

$$\begin{cases} \frac{d\delta_1}{dt} = \omega_b \Delta\omega_1 \\ J \frac{d\Delta\omega_1}{dt} = P_{1\text{ref}} - P_1 - D\Delta\omega_1 \\ T_u \frac{dU_1}{dt} = Q_{1\text{ref}} - Q_1 + k_u(U_{1\text{ref}} - U_1) \end{cases} \quad (1)$$

where δ_1 and $\Delta\omega_1$ represent the virtual power angle and the angular frequency deviation between the GFM inverter and the synchronized rotating coordinate system, respectively. ω_b represents the rated angular frequency, while J and D denote the virtual inertia and virtual damping of the GFM adopting VSG control, respectively. $P_{1\text{ref}}$ and $Q_{1\text{ref}}$ are the reference active and reactive power, respectively, and P_1 and Q_1 are the active and reactive power output by the GFM inverter. k_u is the reactive loop coefficient, T_u represents the time constant of the reactive power loop, and $U_{1\text{ref}}$ represents the reference voltage of the GFM inverter.

The GFL inverter adopts the PQ control strategy [11], and its output power is denoted as $P_2 + jQ_2$.

For the convenience of analysis, the inner loops of the GFM and GFL inverters are neglected [12], the equivalent circuit of the system is shown in Fig. 1, where \dot{U}_1 , \dot{U}_2

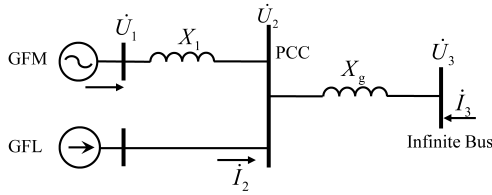


Fig. 1: Equivalent circuit of the system.

and \dot{U}_3 represents the terminal voltage phasor of the GFM inverter, PCC and the AC grid, respectively, and the AC grid is considered as the infinite bus. X_1 , X_2 represents the total impedance from the GFM inverter and the GFL inverter to the PCC respectively, including virtual impedance, step-up transformer impedance, and line impedance. X_g represents the line impedance connecting the PCC to the AC grid. \dot{I}_1 , \dot{I}_2 , and \dot{I}_3 are the node injection currents.

B. TEF of the system

1) *TEF of the GFM inverter:* In order to account for both the Q-V characteristics of the GFM inverter and the

power output characteristics of the GFL inverter, the structure-preserving TEF of the system is introduced based on the energy conservation law as described in [13].

$$W = \int_c \text{Im} \left\{ [(\mathbf{Y}\mathbf{U} - \dot{I}_1 - \dot{I}_2)^*]^T d\mathbf{U} \right\} \equiv 0 \quad (2)$$

where \mathbf{Y} represents the node admittance matrix, \mathbf{U} represents the bus voltage vector, W is the total energy, the integral path c is given by the system trajectory.

By using the theorems in [13] and recalling (1), we can obtain that

$$\begin{aligned} - \int_c I_1^* d\dot{U}_1 &= - \int_{\delta_{1s}}^{\delta_1} P_1 d\delta_1 - \int_{U_{1s}}^{U_1} \frac{Q_1}{U_1} dU_1 \\ &= \int_{\Delta\omega_{1s}}^{\Delta\omega_1} J\omega_b \Delta\omega_1 d\Delta\omega_1 - \int_{\delta_{1s}}^{\delta_1} (P_{1\text{ref}} - D\Delta\omega_1) d\delta_1 \\ &\quad - \int_{U_{1s}}^{U_1} \left(\frac{Q_{1\text{ref}} - k_u U_{1\text{ref}}}{U_1} + k_u - T_u \frac{dU_1}{dt} \right) dU_1 \\ &= \frac{1}{2} J\omega_b (\Delta\omega_1^2 - \Delta\omega_{1s}^2) - P_{1\text{ref}} (\delta_1 - \delta_{1s}) + \int D\omega_b \Delta\omega_1^2 dt \\ &\quad - (Q_{1\text{ref}} + k_u U_{1\text{ref}}) \ln \frac{U_1}{U_{1s}} + k_u (U_1 - U_{1s}) + \int T_u \left(\frac{dU_1}{dt} \right)^2 dt \end{aligned} \quad (3)$$

The subscript s denotes the pre-fault stable equilibrium point (SEP). In order to meet the properties of TEF [14], the TEF of the GFM inverter can be defined as

$$\begin{aligned} V_{\text{GFM}} &= \frac{1}{2} J\omega_b (\Delta\omega_1^2 - \Delta\omega_{1s}^2) - P_{1\text{ref}} (\delta_1 - \delta_{1s}) \\ &\quad - (Q_{1\text{ref}} + k_u U_{1\text{ref}}) \ln \frac{U_1}{U_{1s}} + k_u (U_1 - U_{1s}) \end{aligned} \quad (4)$$

2) *TEF of the GFL inverter:* The GFL inverter is treated as variable load since its internal dynamics are challenging to describe. Therefore, the TEF of the GFL inverter can be written as

$$V_{\text{GFL}} = - \int_c \dot{I}_2^* d\dot{U}_2 = - \int_{\theta_{2s}}^{\theta_2} P_2 d\theta_2 - \int_{U_{2s}}^{U_2} \frac{Q_2}{U_2} dU_2 \quad (5)$$

where θ_2 represents the voltage angle of the PCC. This term can be obtained using trapezoidal integral of the faulty trajectory.

3) *TEF of the network:* The inverter is filtered by an LCL filter and connected to the grid through a step-up transformer. Since the line resistance is significantly smaller than the inductance, the resistance component is neglected, i.e., $\mathbf{Y} = j\mathbf{B}$, \mathbf{B} is the node susceptance. The TEF of the network has been derived in detail in [13], [14] and is directly applied here:

$$\begin{aligned}
V_{\text{BUS}} &= \int_c [(\mathbf{Y}\mathbf{U})^*]^T d\mathbf{U} \\
&= -\frac{1}{2} \sum_{i=1}^3 B_{ii}(U_i^2 - U_{is}^2) \\
&\quad - \frac{1}{2} \sum_{i=1}^3 \sum_{j \neq i}^3 B_{ij}(U_i U_j \cos \theta_{ij} - U_{is} U_{js} \cos \theta_{ijs})
\end{aligned} \tag{6}$$

where θ_i ($i = 1, 2, 3$) represents the voltage angle of each node, subscription i and j represents the number of nodes, $\theta_{ij} = \theta_i - \theta_j$.

C. Proof of Monotonicity of TEF

Combined with the above derivation, the total TEF of the system can be expressed as

$$V = V_{\text{GFM}} + V_{\text{GFL}} + V_{\text{BUS}} \tag{7}$$

By recalling (2), the following transformations can be made:

$$\begin{aligned}
V &= V - W \\
&= V_{\text{GFM}} - \left(-\int_c I_1^* d\dot{U}_1\right) + V_{\text{GFL}} - \left(-\int_c I_2^* d\dot{U}_2\right) \\
&\quad + V_{\text{BUS}} - \int_c [(\mathbf{Y}\mathbf{U})^*]^T d\mathbf{U} \\
&= -\int D\omega_b \Delta\omega_1^2 dt - \int T_u \left(\frac{dU_1}{dt}\right)^2 dt
\end{aligned} \tag{8}$$

The derivative of the TEF with respect to time is

$$\frac{dV}{dt} = -D\omega_b \Delta\omega_1^2 - T_u \left(\frac{dU_1}{dt}\right)^2 \leq 0 \tag{9}$$

It can be obtained that V satisfies the conditions of the energy function and can be used as the TEF of the system. To provide a clearer physical interpretation of the TEF, it is expressed as the sum of kinetic energy V_k and potential energy V_p , where

$$\begin{cases} V_k = \frac{1}{2} J\omega_b (\Delta\omega_1^2 - \Delta\omega_{1s}) \\ V_p = \bar{V} - V_k \end{cases} \tag{10}$$

III. CCT ESTIMATION USING THE IMPROVED IPEBS METHOD

After constructing the TEF of the system, this paper employs the improved IPEBS method [14] to evaluate the CCT following a specific fault. To prevent calculation errors from temporarily exceeding the dot product criterion and prematurely terminating the algorithm—resulting in overly conservative outcomes—this paper modifies the IPEBS method by introducing additional judgment conditions. The specific steps are as follows:

1) Calculate the pre- and post-fault SEP, set the initial number of iterations $n = 0$.

2) Numerically integrate the system during the fault and project the fault trajectory into the post-fault period.

3) Calculate the system energy using (4), (5), (6), (10) by substituting the projected quantities. To avoid misjudgment, set a threshold ε ; compute the dot product criterion until it exceeds ε , then record the energy at this point as $V_c^{(n)}$. The dot product criterion is expressed as

$$f = (P_{1\text{ref}} - P_1) \cdot (\delta_1 - \delta_{1s}) \tag{11}$$

4) Integrate the trajectories under sustained fault conditions, calculating the system energy until $V > V_c^{(n)}$. Record the corresponding time as $t_c^{(n)}$.

5) Clear the fault at $t_c^{(n)}$ and integrate T s for the post-fault system. If $f > \varepsilon$ during this period, proceed to Step 6); otherwise, continue to Step 5).

6) Continue to integrate the system for T_1 s, if $f > \varepsilon$ during T_1 s, proceed to Step 7), otherwise, continue to Step 5).

7) Set $n = n + 1$; assign $V_c^{(n)}$ to the current potential energy value, calculate $t_c^{(n)}$ based on the sustained fault trajectory, and return to Step 5).

8) Output the critical energy $V_c^{(n)}$, with the CCT = $t_c^{(n)}$.

Based on prior experience, the CCT is typically obtained after 1 to 3 iterations. Additional judgment condition Step 6) prevents f from temporarily exceeding the threshold and prematurely terminating the algorithm. The IPEBS method adjusts the optimistic estimate from the PEBS method to a conservative one through a limited number of simulations of the post-fault system. The flow chart is shown in Fig. 2, the revised part of the IPEBS method is shown in red box.

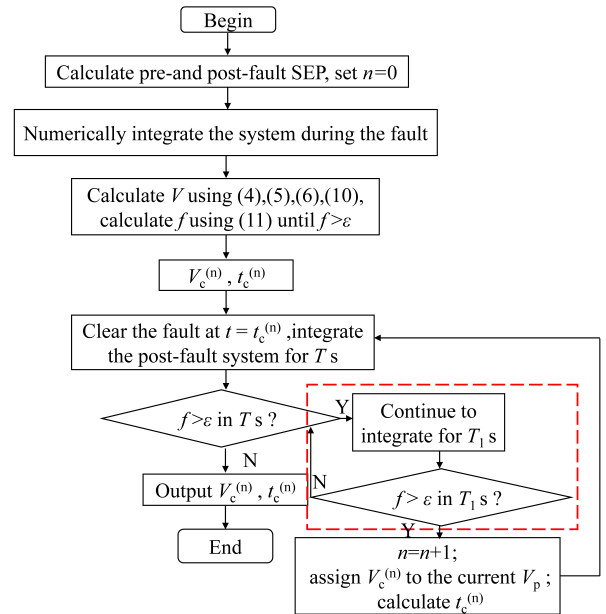


Fig. 2: Flow chart of the improved IPEBS method.

IV. CASE STUDIES

A. Simulation and Verification

To validate the effectiveness of the methodology, a simulation model, as depicted in Fig. 1, was developed using Matlab/Simulink. The system parameters are detailed in the Table I.

TABLE I: System Parameters

Symbol	Description	Value (p.u)
S_1	Capacity of GFM	1
$P_{1\text{ref}}$	Reference active power of GFM	1
ω_b	Angular frequency reference	100π
J	Virtual inertia of GFM	4
D	Virtual damping of GFM	2
$Q_{1\text{ref}}$	Reference reactive power of GFM	0
$U_{1\text{ref}}$	Reference voltage amplitude of GFM	1.1
T_u	Time constant of reactive loop of GFM	10
k_u	Reactive loop coefficient of GFM	10
S_2	Capacity of GFL	1
$P_{2\text{ref}}$	Reference active power of GFL	1
$Q_{2\text{ref}}$	Reference reactive power of GFL	0
$k_{p,\text{pll}}$	Proportional of PLL	100
$k_{i,\text{pll}}$	Integral of PLL	200
X_1	Total impedance from GFM to PCC	0.1
X_g	Total impedance from PCC to AC grid	0.3

A three-phase short-circuit fault is introduced at the PCC with a transition impedance $Z_f = j0.1$ p.u. The dot product criterion threshold $\varepsilon = 10e^{-6}$ and post-fault integration time $T = 10$ s are set. The results from the first iteration of the IPEBS method are shown in Fig. 3a; at this stage, the system destabilizes, and the dot product criterion f oscillates and diverges. As seen in Fig. 3a, when f first crosses ε , the corresponding V_p reaches its initial peak value, with $t = 0.42$ s at that point. The final iteration results are displayed in Fig. 3b, where f remains below zero and V increases continuously during the fault but decreases monotonically under damping effects after the fault is cleared, with V_p and V_k converting into one another.

The CCT, calculated by the IPEBS method, is $t_c = 0.324$ s. Faults are removed at $t_c = 0.324$ s and $t_c = 0.4$ s, respectively, and phase plane diagrams of the state variables (Fig. 4) show that the former system returns to the SEP, while the latter destabilizes. Compared with the CCT of 0.334 s obtained from time-domain simulation, the IPEBS method demonstrates an error of approximately -3%, verifying its accuracy and conservatism, while significantly enhancing computational efficiency over time-domain simulation.

B. Comparative Analysis

To verify the universality of the method, other parameters in Table I were held constant while the grid strength (quantified with $Y_g = 1/X_g$), fault type (Z_f is resistive or inductive), fault severity, and GFL capacity were varied to create different operating scenarios. For each scenario, the CCT was calculated

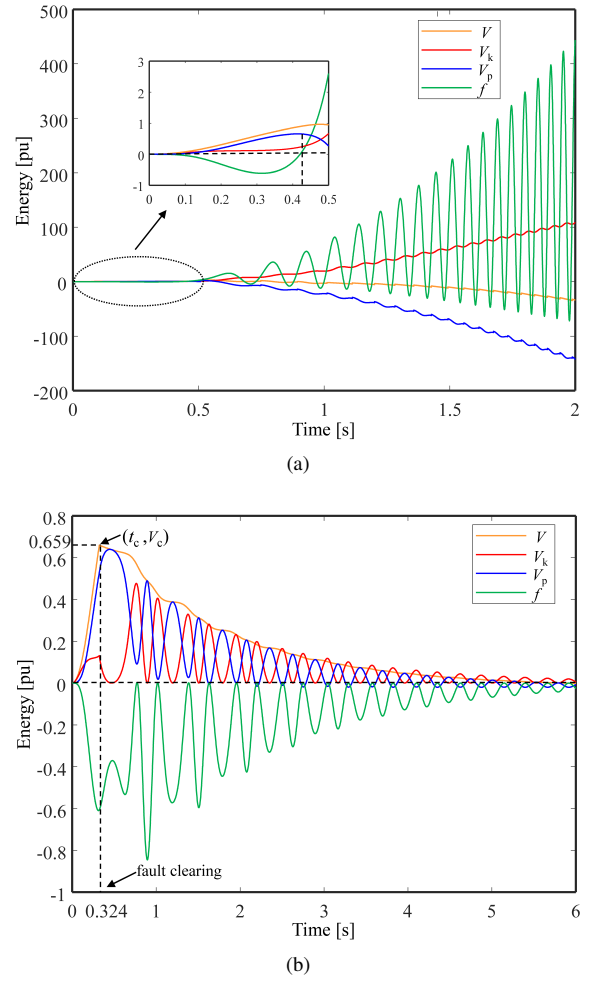


Fig. 3: System energy and dot product criterion curves. (a) In case of system destabilization. (b) In case of system stabilization.

using both the IPEBS method and the improved IPEBS method presented in this paper, denoted as CCT 1 and CCT 2, and these were compared with the CCT obtained from time-domain simulation (CCT 3), as shown in Table 2. The errors between CCT 1, CCT 3 and CCT 2, CCT 3 were denoted as Error 12 and Error 23 respectively.

Table II shows that the IPEBS method without additional judgment conditions may exceed the dot product criterion temporarily due to computational errors or suboptimal threshold settings, causing premature algorithm termination and overly conservative CCT estimates. In contrast, the improved IPEBS method in this paper provides conservative CCT estimates across varied system parameters, fault types, and fault severity scenarios, with an average error of -8.72% relative to time-domain simulation. This improved method significantly reduces conservatism and computational errors compared to the traditional IPEBS method. Additionally, it achieves a computational efficiency over ten times greater than time-domain simulation while maintaining conservative CCT estimation.

TABLE II: Comparison of CCT estimation between the IPEBS method, the improved IPEBS method, and time-domain simulation

Common parameters [pu]	Changed parameters [pu]	CCT 1 [s]	CCT 2 [s]	CCT 3 [s]	Error 13 [%]	Error 23 [%]
$ Y_g $	2.5	0.03	0.146	0.148	-79.730	-1.351
	2.8	0.074	0.176	0.194	-61.856	-9.278
	3.3	0.105	0.324	0.334	-68.563	-2.994
$ Y_g =3.3$	$Z_f=0.1$	0.016	0.029	0.036	-55.556	-19.444
	$Z_f=0.2$	0.017	0.049	0.049	-65.306	0.000
	$Z_f=0$	0.065	0.105	0.131	-50.382	-19.618
$ Y_g =2.5$	$Z_f=j0.05$	0.102	0.102	0.108	-5.556	-5.185
	$Z_f=j0.2$	0.159	0.204	0.239	-33.473	-14.519
$ Y_g =3.3, S_2=0.8$	$Z_f=j0.1$	0.524	0.524	0.524	0.000	0.000
	$Z_f=0$	0.002	0.121	0.142	-98.592	-14.789

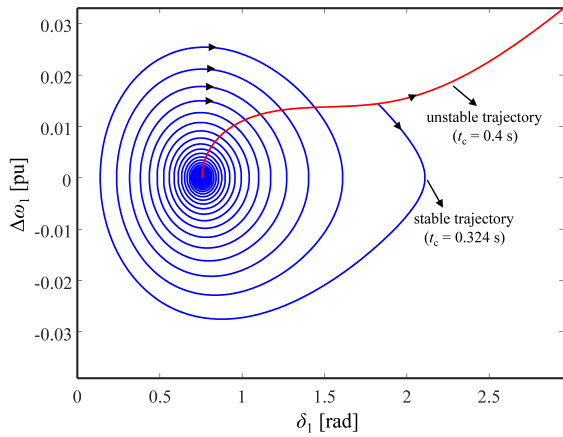


Fig. 4: Phase portraits of $t_c = 0.324$ s and $t_c = 0.4$ s.

Furthermore, the effect on the system's transient stability is analyzed by varying the capacity ratios of the GFM and GFL inverters. With the total delivered power held constant, the capacities of the GFM and GFL inverters are varied, as are the parameters S_1 , S_2 , J , D , and X_1 . Qualitatively, the injection of purely active current of the GFL inverter deteriorates the system's transient stability. Increasing the capacity of the GFM inverter, however, mitigates the GFL's impact on transient stability, enhances inertia support, and optimizes the system's stability, as evidenced by an increase in the CCT shown in Fig. 5. The proposed methodology in this paper demonstrates a trend similar to the time-domain simulation results, all of which are conservative, thereby supporting the generalizability of the method.

V. CONCLUSION

This paper develops a structure-preserving TEF that incorporates the Q-V characteristics of the GFM and the power output characteristics of the GFL, applying the improved

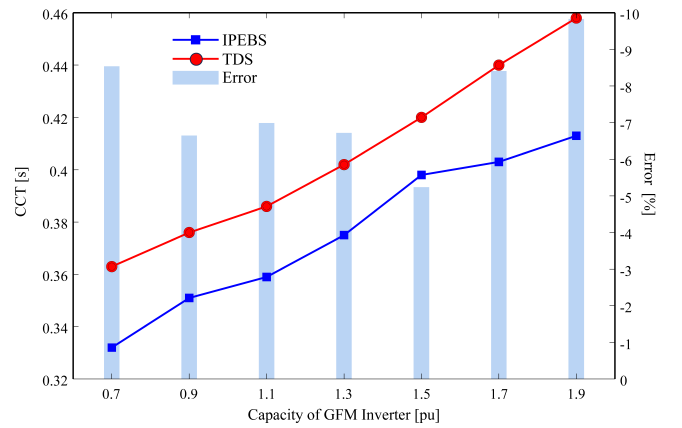


Fig. 5: CCT comparison between IPEBS and TDS methods.

IPEBS method to quickly estimate the CCT of the GFM and GFL inverters integrated system.

Based on the energy conservation law, the reactive voltage characteristics of the GFM and the internal dynamics of the GFL both contribute to transient system stability as components of potential energy. The constructed TEF, verified through theoretical proof and simulation, exhibits a monotonic descent characteristic, meeting transient stability analysis requirements. The proposed improvement to the IPEBS method effectively reduces the conservatism of CCT estimation and avoids CCT misjudgment caused by computational errors or inappropriate threshold settings. Comparison with time-domain simulations demonstrates that the method conservatively estimates CCT, with an average error of -8.72% across various operating scenarios and a computational efficiency over ten times higher, meeting the requirements for online transient stability analysis. This paper also analyzes and verifies the impact of capacity ratio on the system's transient stability.

Future research will consider inverter control switching, such as amplitude limiting and low-voltage ride-through, and

the integration of distributed phase-shifting devices and other reactive power compensation equipment to enhance the system model. This study approximates the GFL inverter as a load and derives its energy function via trapezoidal integration, which inevitably introduces some computational errors. Establishing a path-independent energy function that accommodates multiple dynamic processes will also be a key focus for future research.

ACKNOWLEDGMENT

This work was supported by Zhejiang Provincial Natural Science Foundation of China under Grant No. LY22E070006 and Science and Technology Program of China Southern Power Grid No. ZBKJXM20232475.

REFERENCES

- [1] F. Blaabjerg, R. Teodorescu, M. Liserre, and A. V. Timbus, "Overview of control and grid synchronization for distributed power generation systems," *IEEE Transactions on industrial electronics*, vol. 53, no. 5, pp. 1398–1409, 2006.
- [2] P. Liu, X. Xie, and J. Shair, "Adaptive hybrid grid-forming and grid-following control of ibrs with enhanced small-signal stability under varying scr's," *IEEE Transactions on Power Electronics*, vol. 39, no. 6, pp. 6603–6607, 2024.
- [3] J. Rocabert, A. Luna, F. Blaabjerg, and P. Rodriguez, "Control of power converters in ac microgrids," *IEEE transactions on power electronics*, vol. 27, no. 11, pp. 4734–4749, 2012.
- [4] Y. Li, Y. Gu, and T. C. Green, "Revisiting grid-forming and grid-following inverters: A duality theory," *IEEE Transactions on Power Systems*, vol. 37, no. 6, pp. 4541–4554, 2022.
- [5] P. Kundur, "Power system stability," *Power system stability and control*, vol. 10, pp. 7–1, 2007.
- [6] C. Shen, Z. Shuai, Y. Shen, Y. Peng, X. Liu, Z. Li, and Z. J. Shen, "Transient stability and current injection design of paralleled current-controlled vses and virtual synchronous generators," *IEEE Transactions on Smart Grid*, vol. 12, no. 2, pp. 1118–1134, 2020.
- [7] X. He, S. Pan, and H. Geng, "Transient stability of hybrid power systems dominated by different types of grid-forming devices," *IEEE Transactions on Energy Conversion*, vol. 37, no. 2, pp. 868–879, 2022.
- [8] R. Rosso, S. Engelken, and M. Liserre, "Robust stability investigation of the interactions among grid-forming and grid-following converters," *IEEE Journal of Emerging and Selected Topics in Power Electronics*, vol. 8, no. 2, pp. 991–1003, 2020.
- [9] X. Fu, J. Sun, M. Huang, Z. Tian, H. Yan, H. H.-C. Iu, P. Hu, and X. Zha, "Large-signal stability of grid-forming and grid-following controls in voltage source converter: A comparative study," *IEEE Transactions on Power Electronics*, vol. 36, no. 7, pp. 7832–7840, 2020.
- [10] H. Xin, C. Liu, X. Chen, Y. Wang, E. Prieto-Araujo, and L. Huang, "How many grid-forming converters do we need? a perspective from small signal stability and power grid strength," *IEEE Transactions on Power Systems*, 2024.
- [11] D. B. Rathnayake, M. Akrami, C. Phurailatpam, S. P. Me, S. Hadavi, G. Jayasinghe, S. Zabihi, and B. Bahrani, "Grid forming inverter modeling, control, and applications," *IEEE Access*, vol. 9, pp. 114 781–114 807, 2021.
- [12] H. Geng, C. He, Y. Liu, X. He, and M. Li, "Overview on transient synchronization stability of renewable-rich power systems," *High Voltage Engineering*, vol. 48, no. 9, pp. 3367–3383, 2022.
- [13] Y.-H. Moon, B.-H. Cho, Y.-H. Lee, and H.-S. Hong, "Energy conservation law and its application for the direct energy method of power system stability," in *IEEE Power Engineering Society. 1999 Winter Meeting (Cat. No. 99CH36233)*, vol. 1. IEEE, 1999, pp. 695–700.
- [14] H.-D. Chiang, *Direct methods for stability analysis of electric power systems: theoretical foundation, BCU methodologies, and applications*. John Wiley & Sons, 2011.



CERTIFICATE OF ACHIEVEMENT

PRESENTATION CERTIFICATE

PRESENTED TO

Yisheng Cai

From

Zhejiang University

for the paper

Rapid Estimation of CCT for GFM and GFL Inverters Integrated Systems Using the Direct Method

in recognition and appreciation of your contribution made to Panel Session Chair

IEEE EI² 2024 | Shenyang, China | November 29 - December 02, 2024

CONFERENCE CHAIRS

Prof. Hongbin Sun
Taiyuan University of Technology, China
Tsinghua University, China

Prof. Qiuye Sun
Shenyang University of Technology, China



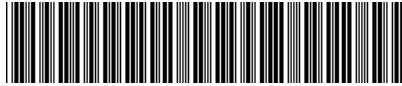
国家知识产权局

310013

浙江省杭州市西湖区古墩路 701 号紫金广场 B 座 1103 室 杭州求是
专利事务所有限公司
邱启旺(0571-87911726-808)

发文日:

2024 年 05 月 30 日



申请号: 202410688389.7

发文序号: 2024053001434430

专利申请受理通知书

根据专利法第 28 条及其实施细则第 43 条、第 44 条的规定, 申请人提出的专利申请已由国家知识产权局受理。现将确定的申请号、申请日等信息通知如下:

申请号: 2024106883897

申请日: 2024 年 05 月 30 日

申请人: 浙江大学

发明人: 周永智, 蔡一晟, 夏杨红, 韦巍, 辛焕海, 李岩, 蔡宏达, 杨鹏程

发明创造名称: 一种跟网型与构网型变流器并联系统的主导不稳定平衡点求解方法
经核实, 国家知识产权局确认收到文件如下:

权利要求书 1 份 9 页, 权利要求项数: 5 项

说明书 1 份 20 页

说明书附图 1 份 2 页

说明书摘要 1 份 1 页

专利代理委托书 1 份 2 页

发明专利请求书 1 份 5 页

实质审查请求书 文件份数: 1 份

申请方案卷号: 邱-241-138-郭

提示:

1. 申请人收到专利申请受理通知书之后, 认为其记载的内容与申请人所提交的相应内容不一致时, 可以向国家知识产权局请求更正。

2. 申请人收到专利申请受理通知书之后, 再向国家知识产权局办理各种手续时, 均应当准确、清晰地写明申请号。

审查员: 自动受理

联系电话: 010-62356655

审查部门: 初审及流程管理部



200101
2023.03

纸件申请, 回函请寄: 100088 北京市海淀区蓟门桥西土城路 6 号 国家知识产权局专利局受理处收
电子申请, 应当通过专利业务办理系统以电子文件形式提交相关文件。除另有规定外, 以纸件等其他形式提交的文件视为未提交。